energies

MDPI

Article

A Comparative Study on Nucleate Pool Boiling Heat Transfer Performance of Low-GWP R-1336mzz(Z) (SF33) Against High-GWP HT55 for Advanced Cooling Applications

Qadir Nawaz Shafiq [1,2], Aqbal Ahmad [3], Kuo-Shu Hung [4], Liang-Han Chien [1,2,*] and Chi-Chuan Wang [3,*]

[1] Department of Energy and Refrigerating Air-Conditioning Engineering, National Taipei University of Technology, Taipei 10608, Taiwan; qadirnawaz.en08@nycu.edu.tw
[2] Research Center of Energy Conservation for New Generation of Residential, Commercial, and Industrial Sectors, National Taipei University of Technology, Taipei 10608, Taiwan
[3] Department of Mechanical Engineering, National Yang Ming Chiao Tung University, Hsinchu 300, Taiwan; aqbal.en10@nycu.edu.tw
[4] Green Energy & Environment Research Laboratories, Industrial Technology Research Institute, Hsinchu 310, Taiwan; kshung@itri.org.tw
* Correspondence: lhchien@mail.ntut.edu.tw (L.-H.C.); ccwang@nycu.edu.tw (C.-C.W.)

Abstract

The present investigation conducts a comparative analysis of the nucleate pool boiling heat transfer performance of two dielectric fluids, a low-GWP hydrofluoroolefin-based fluid (commercially known as Opteon™ SF33, referred to hereafter as SF33) and a perfluoropolyether-based fluid with a high GWP (commercially known as Galden^{R} HT55, referred to hereafter as HT55) under atmospheric pressure conditions. Pool boiling experiments and visual observations were performed to assess essential performance parameters, such as critical heat flux, heat transfer coefficient, and boiling dynamics. SF33 exhibits enhanced heat transfer performance, achieving markedly higher heat transfer coefficient values at all the heat flux levels and attaining superior critical heat flux relative to HT55. The results show that SF33 provides a consistently higher heat transfer coefficient, reaching approximately 12 W/m^2·K at maximum heat flux, compared to only 6 W/m^2·K for HT55, representing nearly a 100% improvement. The visual observations indicated that reduced surface tension and increased latent heat of vaporization of SF33 facilitate more frequent bubble nucleation and smaller bubble departure, thereby enhancing its boiling performance. Properties of SF33 render it a superior candidate for high-performance cooling systems in data centers and power electronics. The study concludes that SF33 is a more efficient and adaptable fluid for next-generation cooling systems, providing superior heat dissipation and energy efficiency relative to HT55.

Keywords: nucleate pool boiling; heat transfer coefficient; low-GWP; dielectric liquids; R-1336mzz(Z); Opteon^{TM} SF33; Galden^{R} HT55

check for updates

Academic Editor: Mahmoud Bourouis

Received: 29 September 2025
Revised: 17 October 2025
Accepted: 28 October 2025
Published: 30 October 2025

Citation: Shafiq, Q.N.; Ahmad, A.; Hung, K.-S.; Chien, L.-H.; Wang, C.-C. A Comparative Study on Nucleate Pool Boiling Heat Transfer Performance of Low-GWP R-1336mzz(Z) (SF33) Against High-GWP HT55 for Advanced Cooling Applications. *Energies* **2025**, *18*, 5719. https://doi.org/10.3390/en18215719

Copyright: © 2025 by the authors. Licensee MDPI, Basel, Switzerland. This article is an open access article distributed under the terms and conditions of the Creative Commons Attribution (CC BY) license (https://creativecommons.org/licenses/by/4.0/).

1. Introduction

As global attention shifts toward enhancing energy efficiency and supporting environmental sustainability, the transition to low-global-warming-potential (GWP) refrigerants has become a critical focus across various industries. The Kigali Amendment to the Montreal Protocol underscores the need for a gradual reduction in the use of high-GWP hydrofluorocarbons (HFCs), thereby placing increasing pressure on industry players and

researchers alike to identify alternative refrigerants that deliver comparable thermal performance with a significantly lower environmental impact [1]. Among these alternatives, dielectric fluids such as SF33 and HT55 have gained considerable interest as potential solutions for thermal management in sectors like high-power electronics and electric vehicles. Recent studies have highlighted the effectiveness of SF33, particularly in electric vehicle (EV) applications and high-performance computing (HPC) environments, where rapid heat dissipation is essential for preventing overheating and ensuring the stable operation of the systems [2,3].

One area that has seen notable advancements is two-phase immersion cooling, a thermal management approach that leverages the phase change of fluids from liquid to vapor to efficiently dissipate heat. This method is now widely adopted in sophisticated data centers and HPC systems, where increased heat loads require enhanced cooling capabilities. Dielectric fluids, including SF33 and HT55, are particularly valued in these environments for their ability to act as electrical insulators, thus enabling the immersion of electronics without risking short circuits [4,5]. As the demand for effective thermal management increases, these fluids contain potential to handle high heat-fluxes while remaining environmentally friendly has made them vital to the growth of next-generation cooling systems.

In the previous literature, SF33 has demonstrated significant potential, particularly for use in fast-charging electric vehicle battery systems, thanks to its low boiling point and high latent heat of vaporization. A study by Rémi and Juhasz [3] highlighted that SF33 offers superior heat transfer performance compared to conventional fluids like Vertrel™ XF, making it a strong candidate for improving EV battery cooling efficiency. This improvement is critical for applications with high thermal loads, where failure to dissipate the heat quickly could lead to catastrophic outcomes such as battery failure or thermal runaway. Given its properties, SF33 has emerged as one of the most promising low-GWP refrigerants across a range of thermal management applications, from automotive systems to electronics cooling.

Despite the inherent properties of dielectric fluids, cooling performance is not solely reliant on the fluid itself but is also influenced by the characteristics of the heat exchange surfaces. Recent research, including studies by Khan et al. [5] and Doran et al. [4], has shown that modifications to the surface such as the addition of micro-fin arrays, pin fins, and nanostructured coatings a dramatically improve pool boiling performance. These surface enhancements increase the nucleation site density, which, in turn, improves both the heat transfer coefficient and the critical heat flux. Such modifications are crucial for improving the overall efficiency of two-phase immersion cooling, particularly in high-power electronics, where controlling heat is critical for maintaining system performance. Both SF33 and HT55 had been shown to respond positively to these surface modifications, demonstrating improvements in bubble nucleation and delayed critical heat flux onset [4].

Additional research into the role of surface modifications in pool boiling heat transfer indicates that surfaces engineered with micro-structured or sintered features significantly enhance boiling behavior, particularly for highly wetting dielectric fluids like SF33 and HT55. In a review by Sajjad et al. [6], the authors highlighted how surface engineering plays a pivotal role in boosting the heat transfer coefficient. While some surface alterations can negatively affect performance, others, such as micro-fin arrays and pin fins, show potential in improving both the critical heat flux and the heat transfer coefficient, making them essential for thermal management in data centers and HPC systems, where high heat dissipation is necessary to prevent thermal issues.

Although significant progress has been made in enhancing the thermal performance of dielectric fluids, there remains a lack of direct comparison between SF33 and HT55 under identical conditions, particularly at atmospheric pressure. Despite their potential

applicability, comprehensive studies comparing their pool boiling behavior specifically in terms of heat transfer coefficient, nucleation site density, and critical heat flux remain scarce. Previous research on low-GWP refrigerants like R-1233zd(E), R-1234ze(E), and R-1336mzz(E) has highlighted the importance of understanding fluid dynamics and heat transfer in pool boiling systems [7,8]. These studies reinforce the need for further experimental research to directly compare low-GWP refrigerants, optimizing their use in immersion cooling applications.

The current study seeks to bridge this knowledge gap by comparing the pool boiling heat transfer properties of SF33 and HT55 under controlled conditions, evaluating their performance at respective saturation temperatures and atmospheric pressure. Key performance metrics such as heat transfer coefficient and critical heat flux will be assessed to provide critical insights into selecting and applying low-GWP refrigerants in advanced thermal management systems. The conclusion of this research work will contribute to the development of more sustainable, efficient cooling systems for high-power devices and offer valuable information on the role of surface engineering in enhancing dielectric fluid performance in immersion cooling applications.

2. Experimental Setup and Methodology

The experimental data were gathered using a controlled pool boiling setup where heat flux was incrementally increased. A schematic representation of the pool boiling apparatus is shown in Figure 1. The experimental system comprises a test section, which is a horizontally inserted plane copper tube with an outer diameter of 20 mm and an effective heating length of 100 mm as depicted in Figure 2. The test section in the evaporator (a cylindrical stainless-steel vessel) which is connected to a condenser, the temperature in the condenser in maintained with the help of a thermostat tank, a liquid line for the return of condensed working fluid in used to return the condensate, as illustrated in Figure 2. The measuring equipment consists of MX-100 (0–5 V), a DC power supply (0–15 A), an absolute pressure transducer (0–2 MPa), eight T-type thermocouples (−250 to 450 °C), and a computer. The temperature distribution was measured using four thermocouples positioned along the tube's periphery. Two were used in the evaporator to measure liquid side temperatures, and two in the condenser to record vapor side saturation temperatures. A substantial (45 mm) insulating layer was applied to the pipes and vessels that transported the fluid in order to prevent heat from leaking into the atmosphere. A nitrogen air-tightness test was conducted 24 h before the test to ensure that there were no leaks, at a pressure of around 9 bar. The pool boiling tests were conducted for SF33 and HT55 on a plane tube surface. Each data point in the graphs was verified using video recordings for precision. The thermophysical properties of both the working fluids are listed in Table 1.

Table 1. Thermophysical Properties of SF33 and HT55 [3,9,10].

Property	SF33	HT55
Saturation Temperature (°C)	33.4	55
Critical Temperature (°C)	171.3	340
Critical Pressure (kPa)	2900	1500
Density at 25 °C (kg/m^3)	1360	1650
Molecular Weight (g/mol)	164	466
Liquid specific heat at 25 °C (kJ/kg K)	1.20	0.96
Latent Heat of Vaporization (kJ/kg)	169	92
Surface Tension (mN/m)	12.7	14
Liquid Thermal Conductivity (W/m·K)	0.08	0.065
Dielectric Strength (0.1″ gap) (kV)	11.5	40
Liquid Viscosity (μPa·s)	162	120
Global Warming Potential (GWP)	2	10,000
Ozone Depletion Potential	0	0

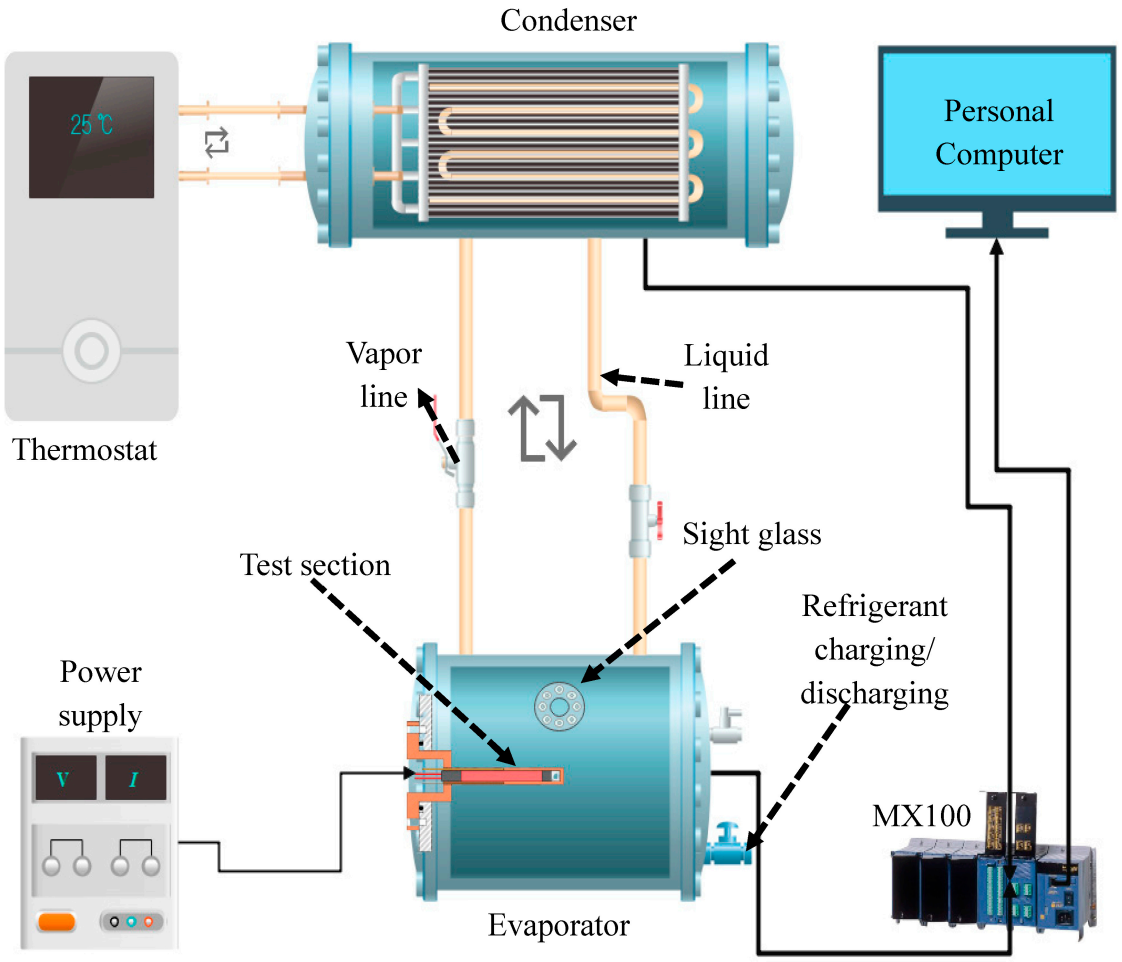


Figure 1. Schematic of the experimental setup used for nucleate pool boiling experimental apparatus.

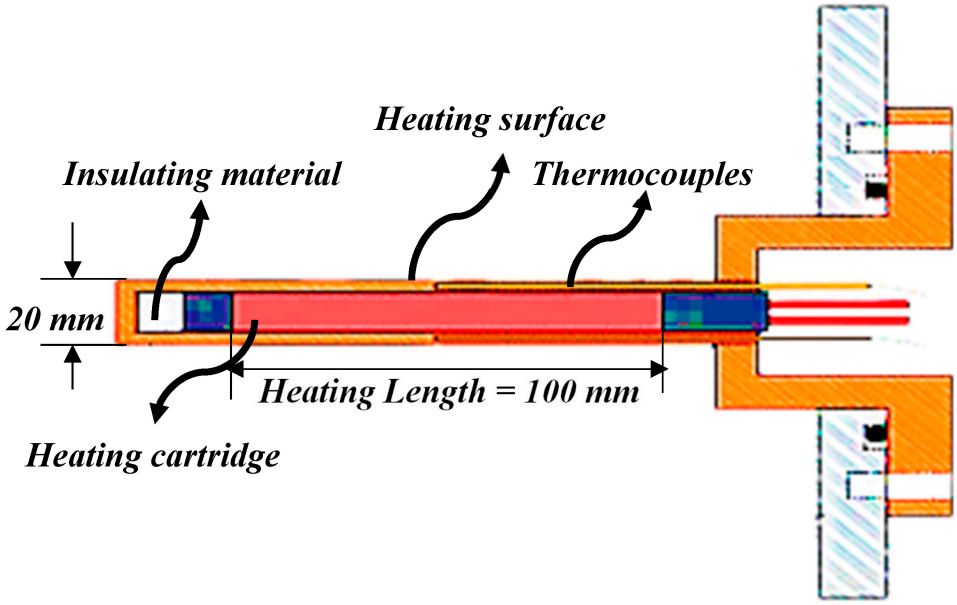


Figure 2. Detailed schematic of test section (a copper smooth tube).

3. Uncertainty Analysis and Data Reduction

The following equation evaluates heat transfer coefficients "h" of SF33 and HT55 on a plane tube surface:

$$h = \frac{q''}{\Delta T} \tag{1}$$

$$\Delta T = T_{tube} - T_{sat} \tag{2}$$

where T_{tube} is surface temperature of the tube, and T_{sat} is the saturation temperature of the working fluids, Q_p is the heat supplied by the heater, q'' is the heat flux, D_o is the outer diameter of the tube, and L is the effective heating length. The wall temperature (T_w) of the tube surface is estimated by the Fourier law:

$$q'' = \frac{Q_p}{\pi D_o L} \tag{3}$$

$$Q_p = Voltage \times Current \tag{4}$$

$$T_w = T_{avg} - Q_p \frac{\ln\left(\frac{D_o}{D_i}\right)}{2\pi KL} \tag{5}$$

where the average temperature, T_{avg}, is determined by four thermocouples placed around the tube circumference. The distance from the location of four thermocouples is denoted by D_i, and k represents the thermal conductivity of the tube material.

The uncertainty in the measurement is determined by the instrument's calibration. The experimental uncertainties are estimated using the uncertainty analysis method as described in the literature [11]. A resistance temperature detector (RTD, Pt-100) with an accuracy of ±0.05 °C was used to calibrate the thermocouples. The voltage and current of the heater cartridge that was inserted into the test section assembly were verified using a digital DC GWINSTEK (GPR-16H50DA) power supply with an uncertainty of 2–5 W. The uncertainty associated with the absolute pressure transducers was ±5 kPa. For parameters like wall superheat $\left(\frac{\delta \Delta T}{\Delta T}\right)$ and heat flux $\left(\frac{\delta q}{q} = \sqrt{\left(\frac{\delta Q_p}{Q_p}\right)^2 + \left(\frac{\delta D_o}{D_o}\right)^2 + \left(\frac{\delta L}{L}\right)^2}\right)$ the uncertainties were 1.25–2.85% and 1–3.33%, respectively. Finally, the uncertainty for heat transfer coefficients $\left(\frac{\Delta h}{h} = \sqrt{\left(\left(\frac{\delta q}{q}\right)^2 + \left(\frac{\delta \Delta T}{\Delta T}\right)^2\right)}\right)$ was estimated to be around 6.8–11.35%.

4. Results and Discussion

Figure 3 shows the heat transfer coefficient vs. wall superheat for the present two working fluids. The SF33 demonstrates a consistent increase in heat transfer coefficient as the heat flux increases, reaching approximately 12 W/m^2·K at the maximal heat flux levels. In contrast, HT55 exhibits a significantly lower heat transfer coefficient than that of SF33, with a maximum of approximately 6 kW/m^2·K at comparable heat flux values. This analysis illustrates that SF33 has a higher heat transfer performance than HT55 at all heat flux levels as it is evident from Figure 4. The higher heat transfer coefficient observed with SF33 is mainly associated with the difference in latent heat. The latent heat for SF33 is nearly 84% higher than that of HT55. As the heat flow increases, the disparity in performance between the two fluids becomes more pronounced. In high heat flux applications, such as power electronics, SF33 maintains efficacy and exhibits enhanced performance, whereas HT55 exhibits symptoms of saturation and inefficiency at elevated heat fluxes. The enhanced heat transfer coefficient demonstrated by SF33 at elevated heat fluxes indicates its greater capacity to manage increased thermal loads. HT55, however,

seems to reach its performance threshold more rapidly, suggesting some limitations in high-demand scenarios.

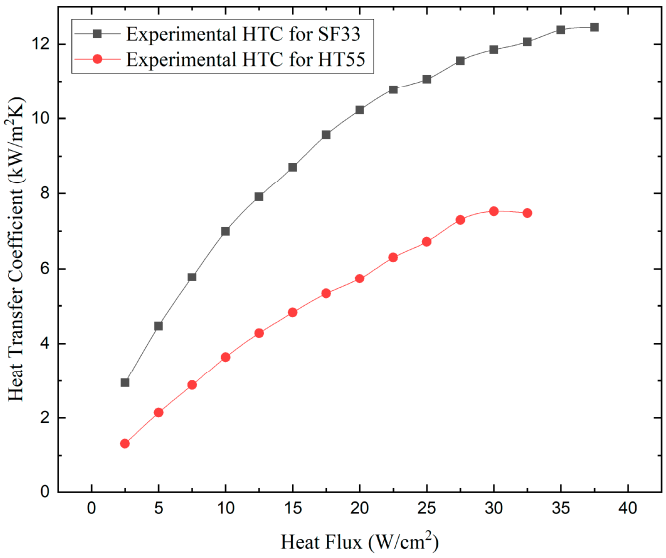


Figure 3. Heat transfer coefficient comparison of SF33 and HT55 at various heat fluxes.

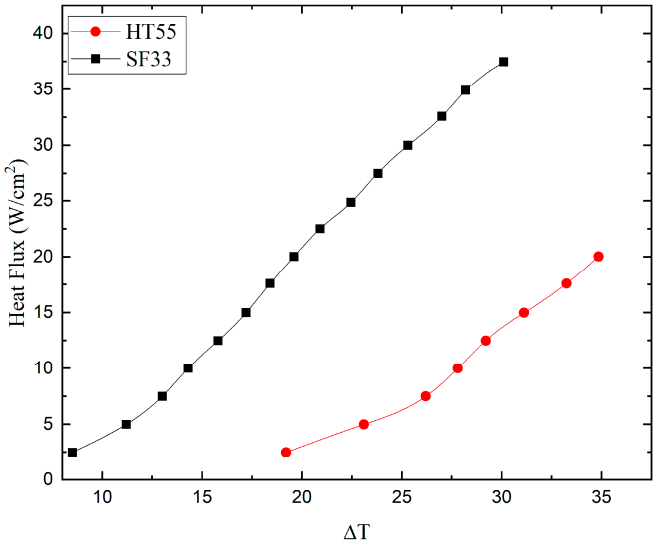


Figure 4. Boiling curve for SF33 and HT55.

In order to validate the experiments the results are compared against three very frequently used heat transfer predicting correlations (i.e., Cooper [12], Ribatski and Jabardo [13], and Jung [14]) as recommended in [8]. Figures 5–7, depict the compression of experimental heat transfer coefficients with predictions across the full heat-flux range. For SF33, Cooper follows the experimental trend and is reasonably close at low–mid heat fluxes, but it remains below the data through most of the range and only converges near the highest q'' (30–35 W/cm^2). For HT55, Cooper consistently overpredicts the heat transfer coefficient with almost parallel slope relative to the measurements. Overall, Cooper's correlation is acceptable for trend comparison with SF33 but is biased high for HT55.

$$HTC_{Cooper} = 90q''^{0.67}M^{-0.5}p_r^m(-Log_{10}p_r)^{-0.55} \quad (6)$$

$$m = 0.12 - 0.2logR_a \quad (7)$$

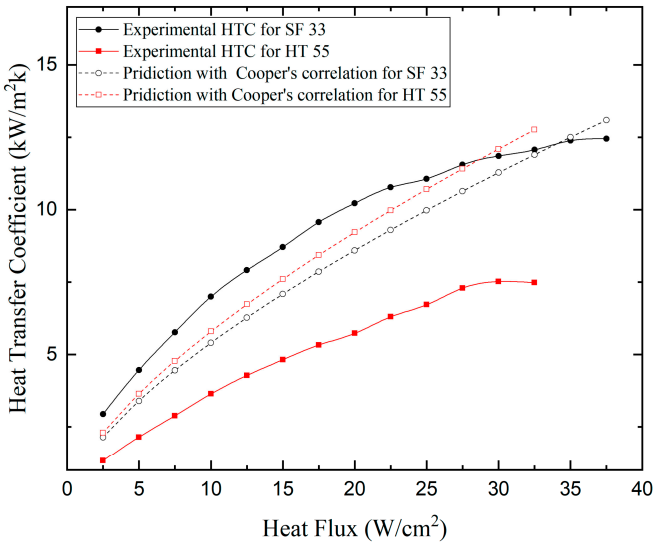


Figure 5. Comparison of Cooper's prediction for SF33 and HT55.

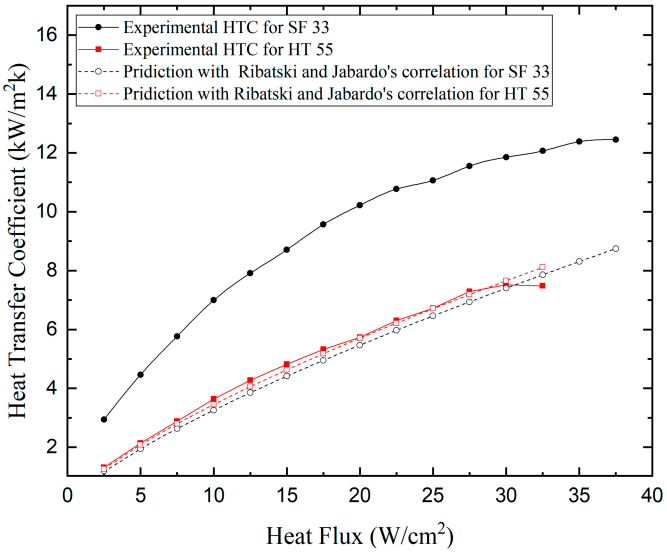


Figure 6. Comparison of Ribatski and Jabardo's prediction for SF33 and HT55.

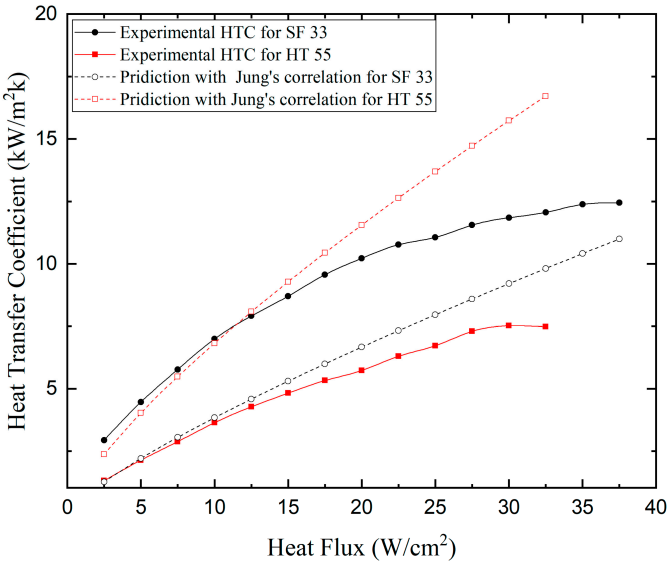


Figure 7. Comparison of Jung's prediction for SF33 and HT55.

Ribatski & Jabardo's correlation tracks HT55 the best predictions follow the experimental slope closely and stay within roughly an experimental increment over most of the range, with only a modest high-end deviation. For SF33, it underpredicts across the entire range by a nearly constant offset (the predicted curve lies below the data with a slightly lower slope). Thus, Ribatski & Jabardo is the most suitable baseline for HT55 in this study, but it is conservative for SF33.

$$HTC_{R\ \&\ J} = 100R_a^{0.2}p_r^{0.45}(-Log_{10}p_r)^{-0.8}M^{-0.5}q''^{(0.9-p_r^{0.2})} \tag{8}$$

Jung's predictions for SF33 are systematically low (increasing underprediction with heat flux), indicating that Jung's formulation, derived for halogenated refrigerants on smooth tubes, does not capture SF33's higher performance. For HT55, the opposite occurs: predictions overshoot the data and the bias grows with q'', suggesting that Jung's pressure/density scaling is not appropriate for this high-molecular-weight dielectric.

$$HTC_{jung} = 41.4\frac{k_l}{d_b}\left(\frac{q''d_b}{k_l T_{sat}}\right)^{-0.835(1-p_r)^{1.33}}(-\log_{10}p_r)^{1.52}\left(1-\frac{\rho_v}{\rho_l}\right)^{0.53} \tag{9}$$

$$d_b = \sqrt{\frac{\sigma}{g(\rho_l-\rho_v)}} \tag{10}$$

Among the tested models, Ribatski & Jabardo best represents HT55, while none of them can well correlate SF33 with small error across all heat fluxes. The Cooper's correlation comes closest in shape but remains low until the highest q''. These results motivate either a tuned coefficient set for these correlations tailored specific to SF33 and HT55 or a compact corrective factor based on reduced pressure and a viscosity/surface tension ratio to reconcile both fluids on the same plain-tube geometry.

The boiling point of SF33 is 33.4 °C, which is considerably lower than HT55's boiling point of 55 °C. The reduced boiling point enables faster boiling and enhanced heat transfer at lower temperatures, providing SF33 with a performance edge in applications necessitating swift heat dissipation. Furthermore, SF33's reduced molecular weight (164 g/mol) in contrast to HT55 (466 g/mol) facilitates its vaporization, enhancing its heat transfer efficacy. The reduced density of SF33 (1360 kg/m^3) and its lower surface tension (12.7 mN/m) relative to density (1650 kg/m^3) of HT55 and surface tension (14 mN/m) further improve its boiling properties. Reduced density and surface tension facilitate more frequent bubble nucleation and expedited evacuation, hence enhancing the overall efficiency of the boiling process. Conversely, HT55's elevated density and surface tension necessitate increased energy for bubble formation and detachment, leading to a diminished heat transfer coefficient. The performance patterns of SF33 indicate a markedly elevated critical heat flux in comparison to HT55.

A fluid with an elevated critical heat flux can accommodate greater heat loads without encountering dryout, a condition where a vapor coating develops on the heating surface, significantly impairing heat transfer. The SF33's enhanced heat transfer coefficient at elevated heat fluxes indicates a greater critical heat flux, rendering it more appropriate for rigorous applications. HT55, conversely, seems to reach its critical heat flux threshold at reduced heat flux levels, limiting its applicability in intense heat dissipation scenarios. It is observed that the SF33 outperforms HT55 across all heat flux levels and temperature differentials due to its superior thermophysical features, including a larger latent heat of vaporization, a lower boiling point, and enhanced density and surface tension. SF33's capacity to attain elevated heat transfer coefficient values and endure increased thermal loads without encountering critical heat flux renders it the ideal selection for high-performance cooling applications, including immersion cooling in data centers and power electronics.

Although HT55 may suffice for less rigorous applications, its diminished heat transfer coefficient and critical heat flux restrict its efficacy in settings necessitating prolonged high heat flux removal.

The boiling characteristics of SF33 and HT55 are visually compared here in Figure 8 as the heat flux increases. The heat transfer performance of both fluids is significantly influenced by the dynamics of bubble nucleation, growth, and departure, which are vividly captured in the images.

Bubble Nucleation and Growth: SF33 exhibits a higher bubble departure frequency and more vigorous bubble nucleation across all heat flux levels. This is a result of the reduced surface tension of SF33 (12.7 mN/m), which facilitates the formation of nucleation sites. Bubbles seem to be more numerous, thinner, and detach from the surface rapidly. The bubbles in HT55 are larger but fewer, and they nucleate more slowly and grow larger before detaching from the heated surface, due to its higher surface tension (17 mN/m). In comparison to SF33, this heat transmission mechanism is less efficient due to the slower nucleation rate.

Bubble Coalescence and Vapor Layer: SF33 facilitates efficient heat transmission throughout the boiling process by maintaining smaller, more frequent bubbles that do not coalesce into large vapor masses as the heat flux increases. This characteristic is crucial for the preservation of a higher critical heat flux, as SF33 prevents the formation of an insulating vapor layer on the surface, even at higher heat fluxes. On the other hand, bubble coalescence is observed in HT55 at increased heat fluxes. The boiling process becomes less efficient as the bubbles become larger and more irregular. Eventually, these coalescing bubbles could create a vapor layer on the surface, which could result in a rapid approach to the critical heat flux and the potential for drying.

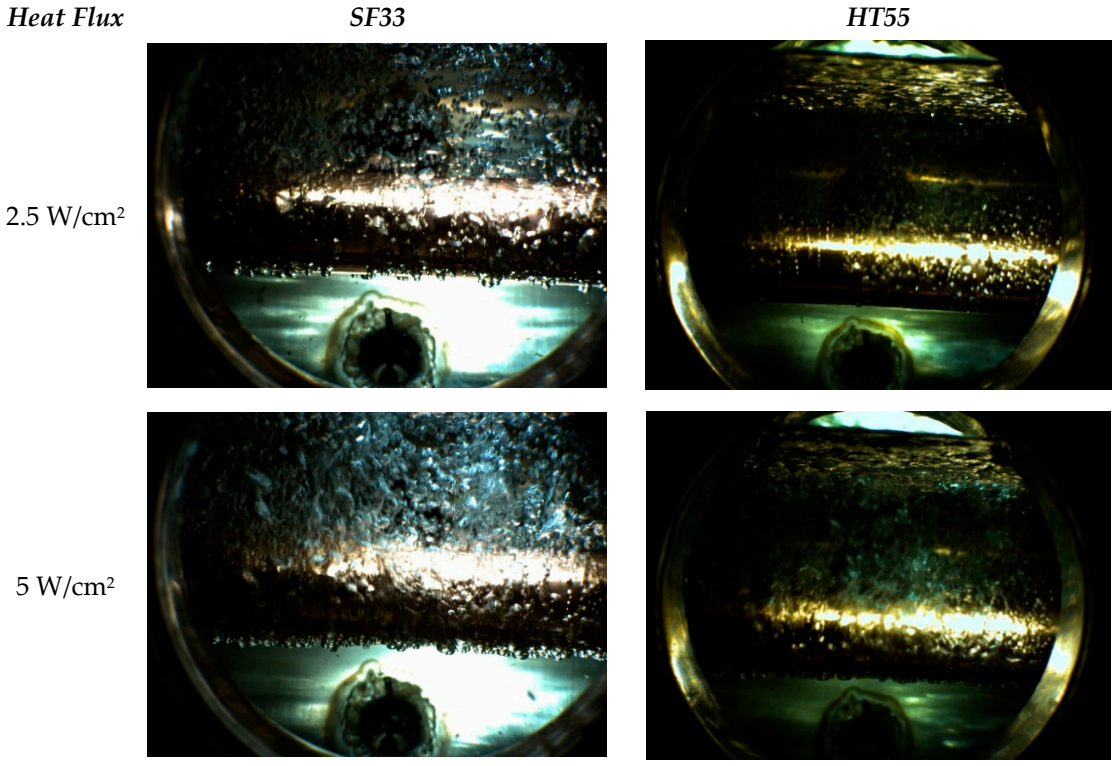


Figure 8. *Cont.*

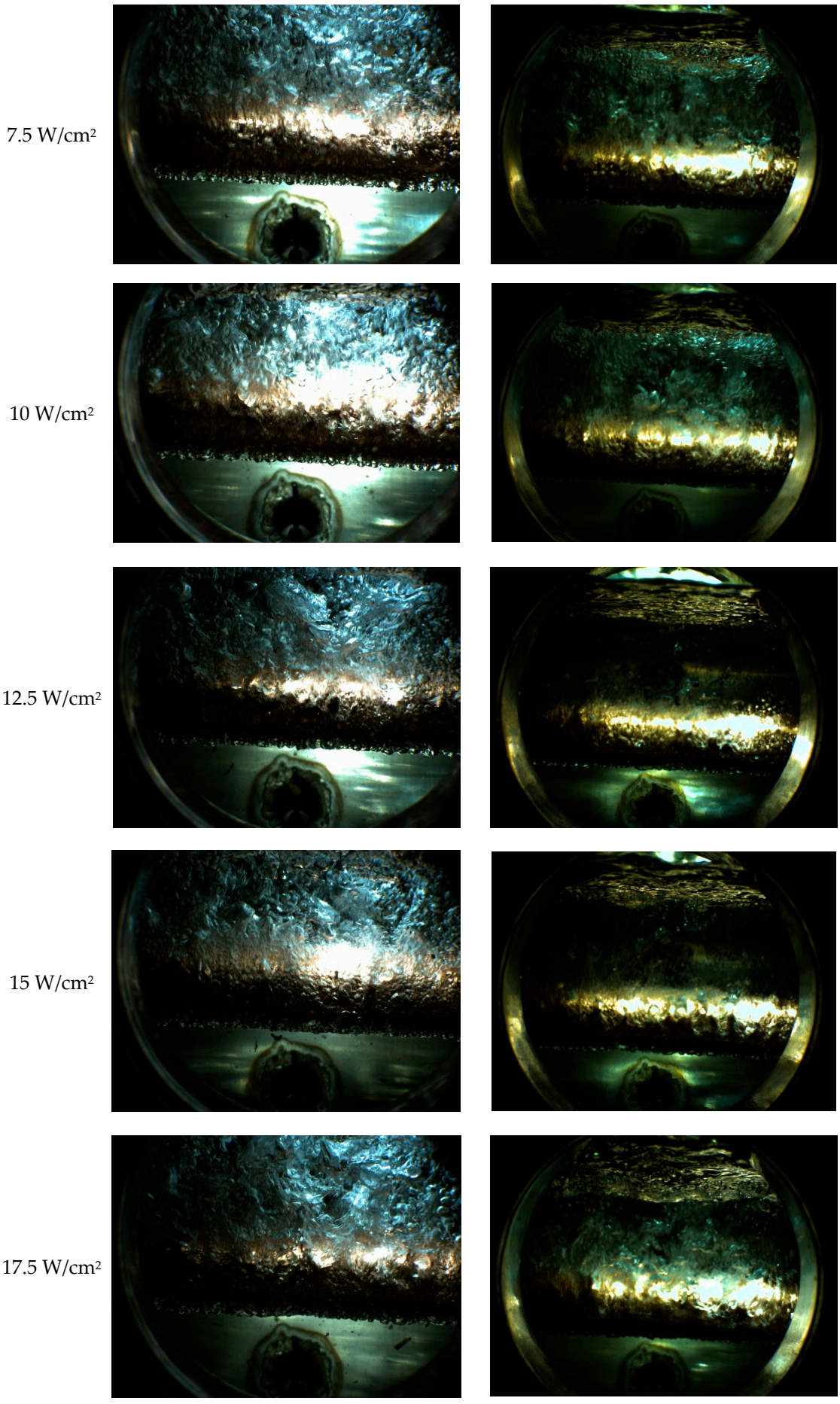


Figure 8. *Cont.*

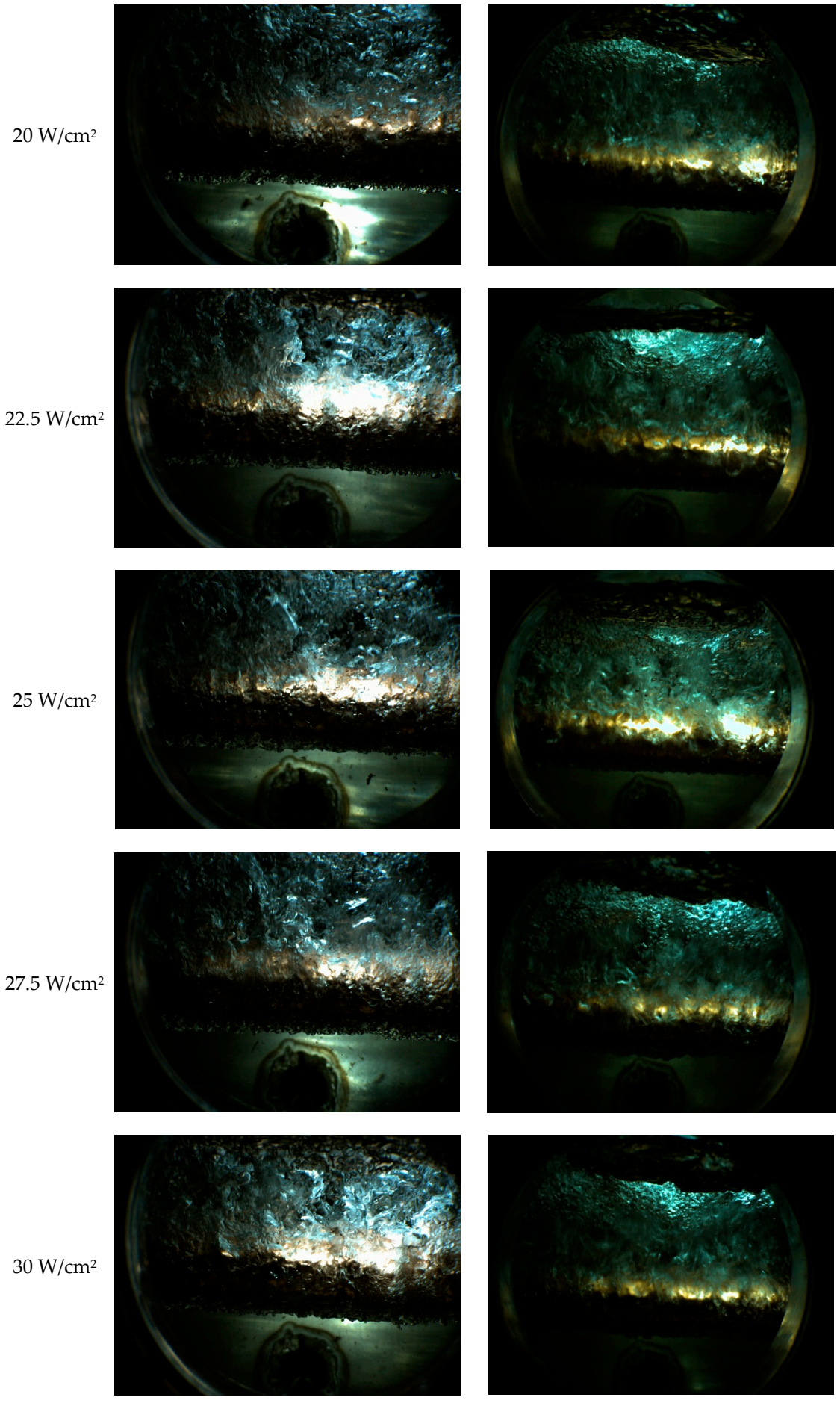


Figure 8. *Cont.*

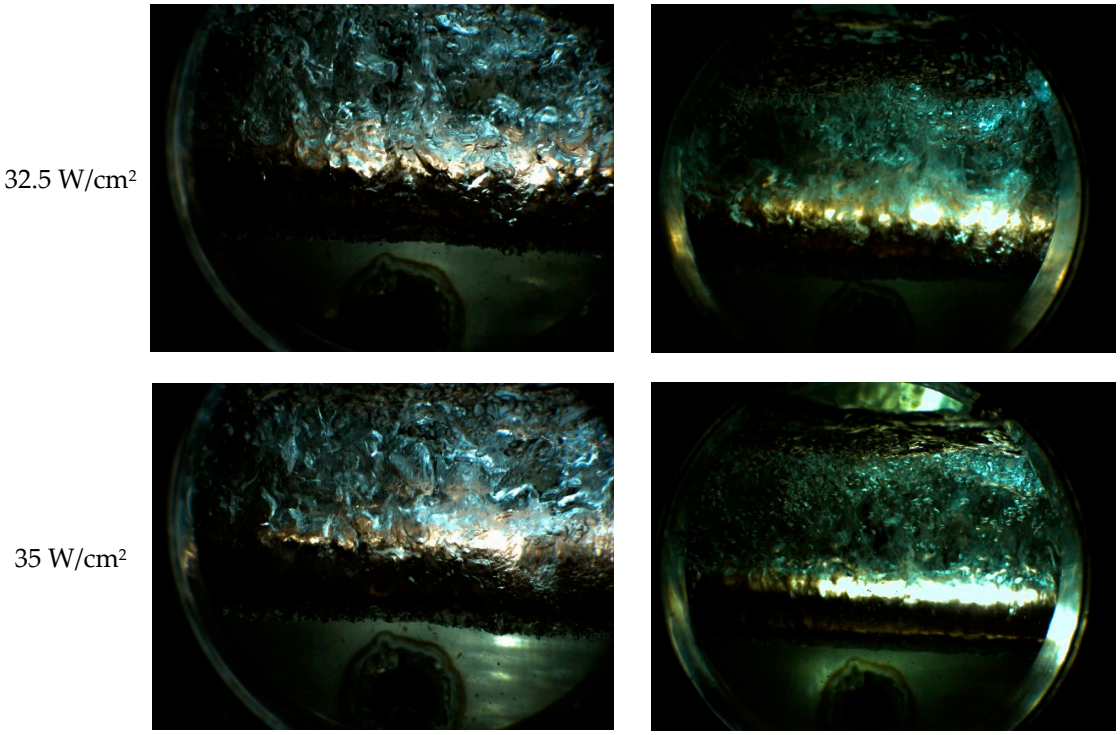


Figure 8. Visualization of boiling behavior for SF33 and HT55 under increasing heat flux.

Film Boiling and Critical Heat Flux Onset: The experimental data is corroborated by the visual analysis, which suggests that SF33 can withstand significantly higher heat flux levels and attain a significantly higher heat transfer coefficient before reaching its critical heat flux. SF33 does not experience substantial film boiling until it reaches significantly higher heat flux levels, and it exhibits well-distributed bubbles. However, the irregular bubble dynamics and the initial formation of vapor regions on the surface provide evidence that HT55 begins to exhibit symptoms of approaching critical heat flux at lower heat fluxes. This is in accordance with the fact that HT55 has a reduced critical heat flux and is unable to withstand sustained high thermal loads without experiencing a substantial performance degradation.

In essence, SF33 has superior boiling efficiency, bubble dynamics, and heat transfer than HT55, making it a better immersion cooling dielectric fluid. Increased heat flow hinders vapor layer formation and bubble coalescence, facilitates rapid bubble departure, and enhances the nucleation rate. HT55 is unsuitable for high-performance applications as it remains stable at lower heat fluxes but begins to deteriorate at elevated levels. In scenarios characterized by significant heat transfer and minimal ΔT, SF33 provides considerable benefits owing to its enhanced versatility and energy efficiency in advanced immersion cooling systems. HT55 is inadequate for high-performance applications. These applications require excellent heat dissipation for system stability and efficiency. SF33 is best for high-performance cooling applications due to its higher critical heat flux and heat transfer coefficient, while HT55 is inappropriate for high-load applications due to its lower heat dissipation.

5. Conclusions

This study conducted a comprehensive comparison of the pool boiling heat transfer performance of SF33 and HT55. The findings indicate that SF33 outperforms in high-performance cooling applications. Quantitative data analysis and visual observations of boiling behavior indicate that SF33 surpasses HT55 regarding heat transfer coefficient

and critical heat flux. SF33 demonstrates a superior capability to maintain a higher heat transfer coefficient at increasing heat flux levels, along with an enhanced critical heat flux, positioning it as a suitable option for applications necessitating efficient heat dissipation, including data centers, high-performance computing (HPC), and power electronics. The thermophysical properties of SF33, including a higher latent heat of vaporization, a lower boiling point, and reduced surface tension, improve its performance by promoting more frequent and efficient bubble nucleation and departure. SF33 exhibits resistance to the formation of insulating vapor layers due to these properties. This indicates its capability to manage elevated thermal loads without a decline in performance or premature attainment of critical heat flux. HT55 demonstrated larger, slower nucleation bubbles and initial indications of vapor coalescence, which constrained its performance at increased heat fluxes. Consequently, applications involving low or moderate heat flux, which emphasize thermal stability and chemical inertness rather than extreme performance, are more appropriate for HT55.

Visual observations further support the enhanced performance of SF33. Under conditions of high heat flux, SF33 exhibited more consistent and efficient phase-change dynamics, preventing the formation of large vapor bubbles and reducing the risk of dryout, which can significantly impair heat transfer efficiency. HT55 reached its operational limits sooner, resulting in the formation and coalescence of larger, slower bubbles at reduced heat fluxes, which suggests an earlier onset of critical heat flux. The implications of this study for the development and optimization of next-generation cooling systems are substantial. SF33 provides an effective solution for immersion cooling applications, emphasizing the importance of optimizing heat transfer performance and ensuring system stability. The ability to adapt to various heat fluxes and temperature differentials enhances its applicability across diverse thermal management systems.

A number of studies indicate that surfaces with micro fins significantly improve heat transfer coefficients and generate smaller diameter bubbles with a higher departure frequency for dielectric fluids like FC-72 and HFE-7100 [15–19]. The results have demonstrated that increasing the number of fins can improve the heat transfer coefficient. Micro-fin surfaces enhance heat transfer at low heat fluxes, with surface shape identified as a crucial determinant. In these articles identified that by reducing fin spacing or increasing fin length may improve the heat transfer coefficient, with the most notable enhancement being five times greater than that of a flat surface. Subsequent research may investigate the efficacy of SF33 and HT55 with various surface modifications or improved boiling surfaces, potentially broadening their applicability. Furthermore, conducting tests under diverse pressures and environmental conditions will yield a comprehensive understanding of the performance of these fluids in practical applications. Considering the growing significance of low-GWP refrigerants in eco-friendly cooling applications, SF33 signifies a noteworthy advancement in sustainable, high-performance thermal management technologies. HT55 is effective in less demanding applications; however, it is unlikely to satisfy the stringent performance standards necessary for high heat flux environments.

In summary, SF33 has demonstrated its efficacy as the optimal dielectric fluid for contemporary thermal management issues. The superior heat transfer coefficient, critical heat flux, and overall boiling performance render it the optimal selection for industries dependent on efficient and reliable cooling solutions. This study's results can guide the design and optimization of advanced cooling systems, enabling engineers to make informed choices regarding working fluids for high-performance environments. The increasing demand for efficient and environmentally sustainable cooling solutions highlights SF33 as a robust, adaptable, and energy-efficient alternative for future thermal management.

Author Contributions: Conceptualization, Q.N.S. and A.A.; Methodology, Q.N.S. and A.A.; Validation, Q.N.S., A.A., L.-H.C. and C.-C.W.; Formal analysis, K.-S.H., L.-H.C. and C.-C.W.; Investigation, Q.N.S., A.A., K.-S.H., L.-H.C. and C.-C.W.; Resources, K.-S.H. and C.-C.W.; Data curation, Q.N.S. and C.-C.W.; Writing—original draft, Q.N.S. and A.A.; Writing—review & editing, Q.N.S., L.-H.C. and C.-C.W.; Visualization, Q.N.S.; Supervision, K.-S.H., L.-H.C. and C.-C.W.; Project administration, L.-H.C. and C.-C.W. All authors have read and agreed to the published version of the manuscript.

Funding: The authors appreciate the major funding from the National Science and Technology Council, Taiwan under contract number 112-2221-E-A49-026. The project was partially supported by the Energy Administration, Ministry of Economic Affairs, Taiwan.

Data Availability Statement: The original contributions presented in this study are included in the article. Further inquiries can be directed to the corresponding author.

Conflicts of Interest: The authors declare no conflicts of interest.

Abbreviations

Nomenclature		*Greek Symbol*	
A	Heated surface area (m^2)	ρ	Density (kg/m^3)
D_o	Outer diameter of tube (m)	μ	Dynamic viscosity (Pa·s)
D_i	Inner diameter of tube (m)	σ	Surface tension (N/m)
d_b	Bubble departure diameter (m)	*Subscripts*	
g	Gravitational acceleration (m/s^2)	b	Bubble
k	Thermal conductivity (W/m·K)	i	Inner
L	Effective heating length (m)	l	Liquid phase
M	Molecular weight (g/mol)	v	Vapor phase
p_r	Reduced pressure	*Sat*	Saturation condition
P_c	Critical pressure (kPa)	w	Wall (outer surface)
q''	Heat flux (W/cm^2)	*avg*	Averaged
Q_p	Electrical heater input power (W)	o	Outer
Ra	Arithmetic mean surface roughness (μm)	*Abbreviations*	
T	Temperature (°C, K)	CHF	Critical heat flux
T_{avg}	Average temperature (°C, K)	GWP	Global warming potential
T_{tube}	Tube surface temperature (°C, K)	HTC	Heat transfer coefficient
T_w	Wall (outer-surface) temperature (°C, K)	HPC	High-performance computing
T_{sat}	Saturation temperature (°C, K)	EV	Electric vehicle

References

1. Shafiq, Q.N.; Liaw, J.-S.; Wang, C.-C. A comprehensive review on the nucleate/convective boiling of low-GWP refrigerants: Alternatives to HFC refrigerants. *Processes* **2023**, *11*, 468. [CrossRef]
2. Heath, E.A. Amendment to the Montreal protocol on substances that deplete the ozone layer (Kigali amendment). *Int. Leg. Mater.* **2017**, *56*, 193–205. [CrossRef]
3. Rémi, D.; Juhasz, J.R. Assessment of immersion cooling fluids for electric vehicle battery thermal management. In Proceedings of the 32nd Electric Vehicle Symposium (EVS32), Lyon, France, 19–22 May 2019.
4. Doran, B.; Zhang, B.; Davani, S.; Osafo, K.A.; Sutka, O.; Walker, A.; Mueller, N.; Akwaboa, S.; Mensah, P.; Meng, W. Spatially periodic vapor bubble activity during subcooled pool boiling on 1D aluminum alloy micro-fin arrays. *Int. J. Heat Mass Transf.* **2021**, *180*, 121760. [CrossRef]
5. Khan, N.; Pinjala, D.; Toh, K. Pool boiling heat transfer enhancement by surface modification/micro-structures for electronics cooling: A review. In Proceedings of the 6th Electronics Packaging Technology Conference (EPTC 2004), Singapore, 8–10 December 2004; IEEE Cat. No. 04EX971.
6. Sajjad, U.; Sadeghianjahromi, A.; Ali, H.M.; Wang, C.-C. Enhanced pool boiling of dielectric and highly wetting liquids–A review on surface engineering. *Appl. Therm. Eng.* **2021**, *195*, 117074. [CrossRef]
7. Kedzierski, M.; Lin, L. Pool Boiling of R514A, R1224 yd (Z), and R1336mzz (E) on a Reentrant Cavity Surface. *J. Heat Transf.* **2021**, *143*, 051602. [CrossRef]

8. Shafiq, Q.N.; Hung, K.-S.; Wang, C.-C. An experimental investigation of nucleate boiling performance for low-GWP azeotropic refrigerant R513A on a smooth tube. *Int. J. Refrig.* **2024**, *162*, 150–157. [CrossRef]
9. McLinden, M.O. *NIST Thermodynamic and Transport Properties of Refrigerants and Refrigerant Mixtures-REFROP*; National Institute of Standards and Technology: Boulder, CO, USA, 1998.
10. TMC Industries Inc. Galden® HT PFPE. Available online: https://tmcindustries.com/products/galden-ht-55 (accessed on 3 October 2024).
11. Dewangan, A.K.; Kumar, A.; Kumar, R. Nucleate Pool Boiling Heat Transfer of Refrigerants Using Coated Surfaces. In *Advanced Cooling Technologies and Applications*; IntechOpen Limited: London, UK, 2019; p. 85.
12. Cooper, M. Heat flow rates in saturated nucleate pool boiling-a wide-ranging examination using reduced properties. In *Advances in Heat Transfer*; Elsevier: Amsterdam, The Netherlands, 1984; pp. 157–239.
13. Ribatski, G.; Jabardo, J.M.S. Experimental study of nucleate boiling of halocarbon refrigerants on cylindrical surfaces. *Int. J. Heat Mass Transf.* **2003**, *46*, 4439–4451. [CrossRef]
14. Jung, D.; An, K.; Park, J. Nucleate boiling heat transfer coefficients of HCFC22, HFC134a, HFC125, and HFC32 on various enhanced tubes. *Int. J. Refrig.* **2004**, *27*, 202–206. [CrossRef]
15. Cao, Z.; Liu, B.; Preger, C.; Wu, Z.; Zhang, Y.; Wang, X.; Messing, M.E.; Deppert, K.; Wei, J.; Sundén, B. Pool boiling heat transfer of FC-72 on pin-fin silicon surfaces with nanoparticle deposition. *Int. J. Heat Mass Transf.* **2018**, *126*, 1019–1033. [CrossRef]
16. Guglielmini, G.; Misale, M.; Schenone, C. Boiling of saturated FC-72 on square pin fin arrays. *Int. J. Therm. Sci.* **2002**, *41*, 599–608. [CrossRef]
17. Kiyomura, I.S.; Nunes, J.M.; de Souza, R.R.; Gajghate, S.S.; Bhaumik, S.; Cardoso, E.M. Effect of microfin surfaces on boiling heat transfer using HFE-7100 as working fluid. *J. Braz. Soc. Mech. Sci. Eng.* **2020**, *42*, 366. [CrossRef]
18. Wei, J.; Honda, H. Effects of fin geometry on boiling heat transfer from silicon chips with micro-pin-fins immersed in FC-72. *Int. J. Heat Mass Transf.* **2003**, *46*, 4059–4070. [CrossRef]
19. Yu, C.K.; Lu, D.C. Pool boiling heat transfer on horizontal rectangular fin array in saturated FC-72. *Int. J. Heat Mass Transf.* **2007**, *50*, 3624–3637. [CrossRef]

Disclaimer/Publisher's Note: The statements, opinions and data contained in all publications are solely those of the individual author(s) and contributor(s) and not of MDPI and/or the editor(s). MDPI and/or the editor(s) disclaim responsibility for any injury to people or property resulting from any ideas, methods, instructions or products referred to in the content.